Liu *et al. Microbiome* (2025) 13:75
https://doi.org/10.1186/s40168-025-02047-4

Microbiome

RESEARCH

Open Access

Short-term and long-term high-fat diet promote metabolic disorder through reprogramming mRNA m^{6}A in white adipose tissue by gut microbiota

Youhua Liu[1,2,3,4†], Jiaqi Liu[1,2,3,4†], Ruiti Ren[1,2,3,4], Zimeng Xin[1,2,3,4], Yaojun Luo[1,2,3,4], Yushi Chen[1,2,3,4], Chaoqun Huang[1,2,3,4], Yuxi Liu[1,2,3,4], Tongyudan Yang[1,2,3,4] and Xinxia Wang[1,2,3,4*]

Abstract

Background Although short-term high-fat diet (S-HFD) and long-term high-fat diet (L-HFD) induce metabolic disorder, the underlying epigenetic mechanism is still unclear.

Results Here, we found that both 4 days of S-HFD and 10 weeks of L-HFD increased mRNA m^{6}A level in epididymal white adipose tissue (eWAT) and impaired metabolic health. Interestingly, S-HFD activated transposable elements (TEs), especially endogenous retroviruses (ERVs) in eWAT, while L-HFD activated long interspersed elements (LINEs). Subsequently, we demonstrated that both S-HFD and L-HFD increased m^{6}A level of *Ehmt2* and decreased EHMT2 protein expression and H3K9me2 level, accounting for activation of ERVs and LINEs. Overexpression of EHMT2 in eWAT or inhibition of ERVs and LINEs by antiviral therapy improved metabolic health under HFD feeding. Notably, we found that both short-term and long-term HFD feeding increased Fimicutes/Bacteroidota ratio and decreased the gut microbiome health index. Fecal microbiota transplantation (FMT) experiments demonstrated that gut microbiota from S-HFD and L-HFD was responsible for increased m^{6}A level in eWAT, resulting in glucose intolerance and insulin insensitivity. Furthermore, we identified that both S-HFD and L-HFD increased the abundance of the gut microbial metabolite homogentisic acid (HGA), and HGA level was positively correlated with unclassified_f__Lachnospiraceae which was both increased in S-HFD and L-HFD feeding mice. Administration of HGA increased the m^{6}A level of *Ehmt2* and decreased the EHMT2 protein expression and H3K9me2 level in eWAT, leading to metabolic disorder in mice.

Conclusions Together, this study reveals a novel mechanism that S-HFD and L-HFD induce metabolism disorder through gut microbiota-HGA-m^{6}A-*Ehmt2*-ERV/LINE signaling. These findings may provide a novel insight for prevention and treatment of metabolism disorder upon short-term or long-term dietary fat intake.

Keywords High-fat diet, Metabolic disorder, m^{6}A, EHMT2, ERVs, LINEs, Gut microbiota, Homogentisic acid

†Youhua Liu and Jiaqi Liu contributed equally to this work.

*Correspondence:
Xinxia Wang
xinxiawang@zju.edu.cn
Full list of author information is available at the end of the article

Background

White adipose tissue (WAT), including inguinal white adipose tissue (iWAT) and epididymal white adipose tissue (eWAT), traditionally thought to be simply a lipid storage site, is now widely recognized as a dynamic organ involved in energy metabolism [1]. In response to high-fat diet (HFD) feeding, WAT expands dramatically, involving both an increase in the size of adipocytes (hypertrophy) as well as an increase in de novo adipogenesis (hyperplasia) [2]. iWAT and eWAT differ in their developmental origin, anatomical location, and response to metabolic stimuli, in which eWAT serve as one of the most obesity-responsive tissues in mice. In response to obesity, eWAT expands dramatically and exhibits fibrosis and chronic inflammation, whereas these phenomena are not largely manifested in iWAT [3]. Numerous studies reported that even short-term (3–7 days) HFD feeding results in impaired glucose uptake in WAT as well as systemic insulin resistance [4–6]. In contrast, long-term intake of HFD feeding leads to chronic inflammation, insulin resistance, and obesity [7]. Despite studies demonstrated that both short-term HFD (S-HFD) and long-term of HFD (L-HFD) cause metabolism disorder, the underlying mechanism is still limited.

Accumulating evidence has demonstrated that environmental or nutritional effects can regulate systemic energy metabolism by different epigenetic mechanisms such as histone modifications, as well as DNA methylation [8]. More recently, it has been shown that mRNA m^6A modification, the most abundant RNA methylation in eukaryote, plays a critical role in adipose tissue development and metabolic health [9, 10]. Maternal HFD intake could dynamically programmed mRNA m^6A modifications in adipose and skeletal muscle tissues in offspring [11]. Supplementation of diet with nutrients, such as epigallocatechin-3-gallate and curcumin, have been shown to alter m^6A RNA methylation of adipose and protect from obesity and metabolism disorder [12, 13]. However, the m^6A profiles and function during S-HFD and L-HFD feeding have not been reported.

To explore the underlying mechanism for S-HFD and L-HFD-induced metabolism disorder, mice were fed with low-fat diet (LFD), 4 days of S-HFD or 10 weeks of L-HFD. We found that both S-HFD and L-HFD impaired metabolism health and increased m^6A level in eWAT. Interestingly, compared to LFD, S-HFD decreased the RNA expression of genes related to response to virus as well as increased endogenous retroviruses (ERVs), while L-HFD increased more long interspersed elements (LINEs). Furthermore, S-HFD and L-HFD increased the mRNA m^6A level of *Ehmt2* and decreased EHMT2 protein expression as well as H3K9me2 level, thereby activating ERVs and LINEs, leading to glucose intolerance and insulin resistance. Finally, we revealed that both S-HFD and L-HFD increased the abundance of homogentisic acid, a key gut microbial metabolite, thereby increasing mRNA m^6A level of *Ehmt2* and decreasing the level of EHMT2 protein and H3K9me2 in eWAT, resulting in metabolic disorder. These findings provided a novel insight for prevention and treatment of metabolism disorder upon short-term or long-term dietary fat intake.

Methods

Animals

Six to 8 weeks old C57BL/6 mice in this study were purchased from Shanghai SLAC Laboratory Animal Co., Ltd (SLAC, China). Mice were housed and maintained at 22 ± 2 °C with a humidity of 35 ± 5% with 12 h light and dark cycles and free access to water and food. All research on animal study was carried out under approval of the Ethics Committee of Zhejiang University (ZJU20240321). All animal experiments were performed from March 21 to May 30, 2024.

Diet studies

For a low-fat diet (LFD) group, 6-week-old male C57BL/6 mice were fed LFD (10% fat in calories; Research Diets, D12450J, USA) for 70 days. For short-term high-fat diet (S-HFD) group, 6-week-old male C57BL/6 mice were fed LFD for 66 days and then fed a HFD (60% fat in calories; Research Diets, D12492, USA) for another 4 days. For long-term high fat (L-HFD) group, 6-week-old male C57BL/6 mice were fed a HFD for 70 days. At the end of 70 days of diet studies, GTT and ITT assays were performed to explore the role of gut microbiota on glucose tolerance and insulin sensitivity.

Glucose and insulin tolerance tests

For glucose tolerance test (GTT), mice fasted overnight were intraperitoneally injected with 2 g/kg glucose (Sangon Biotech, China). For insulin tolerance test (ITT), mice fasted overnight were intraperitoneally injected with 0.75 U/kg insulin (Beijing Solarbio Science & Technology, China). Blood glucose level was detected in tail blood at 0, 15, 30, 60, 90, and 120 min after glucose or insulin injection using a glucometer with glucose testing strips.

RNA isolation and m^6A dot blot

Total RNA was extracted with RNAiso Plus reagent (Takara, Japan), then mRNA was isolated using the Dynabeads® mRNA DIRECT™ kit (Thermo Scientific, USA). After denaturing at 65 °C for 5 min, 200 ng mRNA was loaded on a hybond-N^+ membrane (GE Healthcare, USA) and crosslinked by a UV Stratalinke at 1200 μJ twice. The membrane was washed with PBST for 5 min

and blocked with 5% non-fat milk in PBST for 1 h. The membrane was incubated with anti-m^{6}A antibody (Synaptic Systems, #202 003, Germany) overnight at 4 °C and then incubated with secondary antibody at room temperature for 1 h. The membrane was visualized using chemiluminescence (ECL Plus detection system) and stained by 0.1% methylene blue.

Western blot

Total protein was extracted with RIPA buffer (Beyotime Biotechnology, China) containing 1 × protease and phosphatase inhibitor (Beyotime Biotechnology, China). A total of 30 μg protein was loaded into 4–20% PrecastProteinPlusGel (Yeasen Biotechnology, China) and transferred to PVDF membranes (Life Technologies, USA). After blocking in 5% skim milk, the membranes were incubated with primary antibodies overnight at 4 °C, and then incubated with corresponding secondary antibodies for 1 h at room temperature. The antibodies were summarized below: rabbit monoclonal anti-EHMT2 antibody (ABclonal, #A19288, China); rabbit polyclonal anti-Histone H3 antibody (ABclonal, #A2348); rabbit polyclonal anti-H3K9me2 antibody (ABclonal, #A2359, China); rabbit monoclonal anti-beta Actin antibody (Servicebio, #GB15003, China).

Quantitative real-time PCR analysis

Total RNA from cells or tissues were extracted using TRIzol reagent (TAKARA, Japan) and reverse-transcribed into cDNA using M-MLV reverse transcriptase (Thermo Fisher Scientific, USA). qPCR was performed using the SYBR Green PCR Master Mix (VAZYME, China) with the Rio-rad Real-Time PCR System (Bio-rad, USA). The data were analyzed following the $2^{-\Delta\Delta Ct}$ method. The primers were listed as follows. Ehmt2-qPCR-F: 5′-AGC CAAGAGGGGTCTCCAAT-3′; Ehmt2-qPCR-R: 5′-CTC GCTGATGCGGTCAATCT-3.

MeRIP-qPCR

Twenty-microgram RNAs were fragmented at 30 s on, 30 s off, 30 cycles in Bioruptor® Pico. One-tenth of the fragmented RNAs were saved as input control. A total of 0.5 μL m^{6}A antibody (NEB, USA) was incubated with 20 μL Protein G Magnetic beads (NEB, USA) in 200 μL reaction buffer (10 mM Tris–HCl, pH 7.5, 150 mM NaCl, 0.1% IGEPAL in nuclease free water) with orbital rotation at 4 °C for 1 h. After washing beads twice with 250 μL reaction buffer, resuspended with beads with 200 μL reaction buffer and added nine-tenth of the fragmented RNAs incubated. The beads-antibody-RNAs complex was incubated with orbital rotation at 4 °C for 4 h. Washed the beads-antibody-RNAs complex twice with 200 μL reaction buffer, 200 μL low-salt buffer (10 mM Tris–HCl, pH 7.5, 50 mM NaCl, 0.1% IGEPAL in nuclease free water) and 200 μL high-salt buffer (10 mM Tris–HCl, pH 7.5, 500 mM NaCl, 0.1% IGEPAL in nuclease free water) respectively. Finally, RNAs were eluted with RLT buffer (Qiagen, Germany) following ethanol precipitation. The IP and input control RNA were reverse-transcribed with random hexamers, and m^{6}A enrichment was determined by qPCR. The data were analyzed following the $2^{-\Delta\Delta Ct}$ method, and the relative enrichment of m^{6}A in each sample was calculated by normalizing to input. The primers were listed as follows. Ehmt2-MeRIP-qPCR-F: 5′-GGG TGGACTCTGACAGCAAG-3′; Ehmt2-MeRIP-qPCR-R: 5′-GACGTGTCATTGGAGACCCC-3′.

In vivo transfection

pcDNA3.1-Ehmt2-3 × Flag plasmid was injected into the eWAT of 8-week-old male C57BL/6 mice (20 μg/mouse) in the presence of in vivo DNA transfection reagent (Entranster-in vivo; Engreen, China).

Antivirus treatment of mice

Eight-week-old male C57BL/6 mice were provided a 60 mg/kg Emtricitabine (Aladdin, China) as described previously [14]. In detail, antiretroviral drug Emtricitabine was dissolved in water to 7.5 mg/mL, and Emtricitabine was administrated daily by gavage to mice in a total volume 200 μL starting at HFD feeding. After 1 week, GTT and ITT assays were performed to explore the role of gut microbiota on glucose tolerance and insulin sensitivity.

Antibiotic treatment and fecal microbiota transplantation

Antibiotic (Abx) treatment was performed as described previously [15]. Briefly, 8-week-old male C57BL/6 mice were administered an antibiotic cocktail containing ampicillin, neomycin, metronidazole, and vancomycin via oral gavage for 5 days. Fecal microbiota transplantation was performed as described previously [15]. Briefly, fresh feces were collected from LFD, S-HFD, and L-HFD feeding mice at the end of 10 weeks of LFD feeding, 4 days of HFD feeding or 10 weeks of HFD feeding. A total of 100 mg feces were suspended in 1 ml sterile PBS. The suspension was filtered by 80 mesh, 200 mesh and 400 mesh sterile gauze to obtain fecal microbiota suspensions. Abx-treated mice were daily gavaged with 200 μL of fecal microbiota suspensions. All mice were fed with NCD. After 1 week, GTT and ITT assays were performed to explore the role of gut microbiota on glucose tolerance and insulin sensitivity.

HGA treatment of mice

To determine the effects of HGA, 8-week-old male C57BL/6 mice were injected intraperitoneally with PBS

or 250 mg/kg HGA (Sigma) daily for 4 days as described previously [16].

m^{6}A-seq

m^{6}A library construction was performed as previously reported [17]. Briefly, 1 μg mRNA in 100 μL nuclease-free water was fragmented by Bioruptor (30 s on/off for 30 cycles; Diagenode, Belgium). Ten percent of the fragmented mRNA was used as input and the remaining RNA was used for m^{6}A IP using the EpiMark N6-Methyladenosine Enrichment Kit (NEB, USA). Both input and IP samples were used for library construction by using the VAHTS Universal V8 RNA-seq Library Prep Kit (Vazyme, USA). Library sequencing was performed at Azenta Life Sciences (China) on an Illumina NovaSeq machine in pair-end mode with 150 bp per read.

m^{6}A-seq data analysis

Analysis was performed as described previously [18]. Raw reads were trimmed by Trimmomatic (v0.39) [19], and then aligned to the mouse genome (mm10) using STAR (v2.7.10a) [20]. m^{6}A peaks were called using MACS2 (v2.1.1) [21] with the parameter "—nomodel." The m^{6}A peaks were annotated using mouse gene GTF file downloaded from the ENSEMBL database or transposable elements (TEs) GTF file downloaded from TEtranscripts website. Differentially analysis of m^{6}A level was performed using QNB (v1.1.11) [22]. Motif enrichment analysis of m^{6}A peak was performed with HOMER software (v4.11.1) in RNA mode [23], and GO enrichment of m^{6}A-modified genes was performed using clusterProfiler R package [24]. TCseq R package (v1.30.0) was used to perform an unsupervised clustering analysis of m^{6}A-modification as previous study reported [25]. Briefly, m^{6}A level of each peak identified from LFD, S-HFD, and L-HFD were used for unsupervised clustering analysis by TCseq R packages. "cm" was set as the clustering method to generate clusters by using "timeclust" function of TCseq R packages. "z-score" was set to plot the clusters generated from "timeclust" by using timeclustplot function of TCseq R packages.

RNA-seq data analysis

For RNA-seq data analysis, raw reads were trimmed by Trimmomatic (v0.39), and then aligned to the mouse genome (mm10) using STAR (v2.7.10a) with default option. Reads count was calculated by featureCounts (v2.0.1) [26] and differentially analysis was performed by DESeq2 (v1.46.0) [27] with p value < 0.05 and |log2Foldchange| > 0.58. TEs analysis was performed as previously described [28]. Briefly, cleaned reads were aligned to mm10 using STAR (v2.7.10a) with the option –runMode alignReads, –winAnchorMultimapNmax 100, and –outFilterMultimapNmax 100. The abundance of TEs were identified by TEtranscript software (v 2.2.1) [29] with the option –mode multi, –minread 1, and -i 10. GTF files for TE annotation were downloaded from the TEtranscripts website. DESeq2 R package (v1.46.0) was used to perform differentially analysis of TEs with p value < 0.05 and |log2Foldchange| > 1.

16S rRNA sequencing and data analysis

Fresh feces (~ 200 mg) were collected from LFD S-HFD and L-HFD-fed mice. Fecal DNA was extracted from fresh fecal samples using E.Z.N.A.® soil DNA Kit according to the manufacturer's protocols. Specific primers (338F, 5′-ACTCCTACGGGAGGCAGCAG-3′; 806R, 5′-GGACTACHVGGGTWTCTAAT-3′) were used to amplify V3–V4 region of 16S rRNA gene, and the amplification products were sequenced on Illumina MiSeq platform by Majorbio Bio-Pharm Technology Co., Ltd. (Shanghai, China).

Bioinformatic analysis of the gut microbiota was carried out using the Majorbio Cloud platform (https://cloud.majorbio.com). Sequencing reads were clustered into operational taxonomic units (OTUs) using UPARSE (v7.1) with 97% sequence similarity level [30]. RDP Classifier was used to analyze the taxonomy of OTU representative sequence. Based on the OTU information, alpha diversity indices were calculated with Mothur (v1.30.1) [31]. The similarity among the microbial communities in different samples was determined by principal coordinate analysis (PCoA) based on Bray–Curtis dissimilarity using Vegan (v2.5–3) package. The linear discriminant analysis (LDA) effect size (LEfSe) (http://huttenhower.sph.harvard.edu/LEfSe) was performed to identify the significantly abundant taxa of bacteria among the different groups (LDA score > 3.5, p < 0.05). The gut microbiota health index (GMH) was calculated as previously reported [32]. Run MetaPhlAn2 on stool metagenome(s) using the "–tax_lev s" argument and merge the MetaPhlAn2 outputs. Open the GMHI.R script and load the merged MetaPhlAn2 output file by providing the appropriate path. Then, run GMHI.R in its entirety.

Untargeted metabolomics analysis

Metabolites from fresh fecal samples collected from LFD S-HFD and L-HFD-fed mice were extracted with buffer (methanol:water, 4:1). The LC–MS/MS analysis of the metabolites was performed by Thermo UHPLC-Q Exactive HF-X system (Thermo Fisher Scientific, USA) at Majorbio Bio-Pharm Technology Co., Ltd. (Shanghai, China). Data analysis was processed by using Progenesis QI (Waters). Bioinformatic analysis of the gut metabolites was carried out using the Majorbio Cloud platform (https://cloud.majorbio.com).

Statistical analysis

Data was presented as means ± SD unless otherwise indicated. Either Student's *t*-test or ordinary one-way ANOVA methods were utilized to determine differences among multiple groups by using GraphPad software. $p < 0.05$ is considered as statistically significant.

Results

Both short-term and long-term HFD feeding induce metabolism disorder and increase m^{6}A level in eWAT

To investigate the role of S-HFD and L-HFD feeding on metabolic health, 4 days of S-HFD and 10 weeks of L-HFD feeding assay (Fig. 1A) were performed. Body weight and body weight gain were increased in L-HFD compared to LFD, and S-HFD (Fig. 1B, C, and S1A). Consistently, the results of food intake showed that daily calorie intake was increased in L-HFD compared to LFD, and S-HFD (Fig. S1B). Moreover, L-HFD, not S-HFD, significantly increased fat ratio and tissue weight of iWAT, eWAT, and liver of mice (Fig. 1D–E and S1C). In addition, both S-HFD and L-HFD feeding increased the adipocyte size of iWAT and eWAT (Fig. 1F). Notably, both S-HFD and L-HFD induced glucose intolerance and insulin insensitivity of mice (Fig. 1G–J), even though the plasma insulin level increased in L-HFD instead of S-HFD compared to LFD (Fig. S1D). Our previous studies indicated that mRNA m^{6}A play important role in metabolism regulation [9, 33]. To explore whether S-HFD and L-HFD feeding could affect the mRNA m^{6}A level of WAT, m^{6}A dot-blot was performed. The results showed that both S-HFD and L-HFD feeding increased the mRNA m^{6}A level in iWAT and eWAT, especially in eWAT (Fig. 1K), suggesting a regulatory role of m^{6}A on eWAT.

Activation of TEs is related to metabolic disorder phenotypes upon short-term and long-term HFD feeding

To investigate gene expression on transcriptome level in eWAT upon LFD, S-HFD, and L-HFD feeding, RNA-seq was performed. Differential gene expression analysis identified 3144 upregulated and 889 downregulated genes in S-HFD group when compared with LFD group (Fig. S1 E). Comparing with LFD group, 869 upregulated and 1165 downregulated genes in L-HFD group were identified (Fig. S1 F). Comparing with S-HFD group, 1577 upregulated and 4133 downregulated genes in L-HFD group were identified (Fig. S1 G). To explore the function of differentially expressed genes, Gene Ontology (GO) enrichment analysis of upregulated and downregulated genes was performed respectively. The results showed that S-HFD increased the expression of genes involving in protein localization to cilium, smoothened signaling pathway and cell cycle regulation (Fig. 2A) when compared with LFD, indicating that abundantly ciliated preadipocytes were activated. Compared with LFD, L-HFD increased the expression of genes involving in cytokine production and extracellular structure organization (Fig. 2B), suggesting an enhanced extracellular remodeling and proinflammatory response. Compared with S-HFD, L-HFD increased the expression of immune response process related genes (Fig. 2C). These findings were similar to previous study that inflammation in eWAT is not apparent after 1 week of HFD [5]. Interestingly, when compared with LFD, S-HFD decreased the expression of genes involving in phagocytosis, response to virus and defense response to bacterium (Fig. 2D), while L-HFD decreased the expression of genes associated with defense response to bacterium, negative regulation of proteolysis, and cofactor metabolic process (Fig. 2E). Not surprisingly, L-HFD impaired cilium-related process when compared with S-HFD (Fig. 2F).

It has been reported that HFD promotes endogenous retrovirus (ERVs) expression in keratinocytes [14], promoting us to ask whether S-HFD would induce transposable elements (TEs), such as ERVs, accounting for the observed response to virus. To characterize the TE expression in eWAT, TE expression analysis based on RNA-seq data was performed. The result showed that S-HFD activated the RNA expression of ERVs, such as MER50, LTR28, and LTR68 (Fig. 2G and S1H). In contrast, L-HFD specificity activated long interspersed elements (LINEs), such as L1Md_Gf, L1Md_F, and L1M3f (Fig. 2H and S1I). In total, 20 and 8 TEs with upregulation and downregulation in eWAT upon S-HFD feeding were identified. Twenty-three and 13 TEs with upregulation and downregulation in eWAT upon L-HFD feeding were found. Notably, LTR and LINE were the majority upregulation TEs in S-HFD and L-HFD fed mice, respectively (Fig. 2I). Recently, TEs have been gaining increasing attention due to their regulatory roles in gene expression, in which TEs influence transcriptional activity of nearby genes by providing binding sites for transcription factors (TFs) [34]. To identify the potential TFs interacted with those increased TEs, TEs–TFs association analysis by using RTFAdb, a public repository of the overrepresented TFs in the binding sites of the human and mouse TFs [35], was performed. The results indicated that TFs, such as EP300, TAL1, TCF12, and ZNF384, were significantly associated with MER50, an overrepresented retrotransposon in S-HFD fed mice, while MAFK and ZNF384 were significantly associated with L1Md, which was upregulated in L-HFD fed mice (Fig. 2J). To ask whether those TFs were related to metabolism regulation, Human Genetic Evidence (HuGE) Score of EP300 and MAFK were calculated in T2D Knowledge Portal (T2DKP) website [36]. The results showed that EP300 showed very strong evidence to type 2 diabetes (T2D),

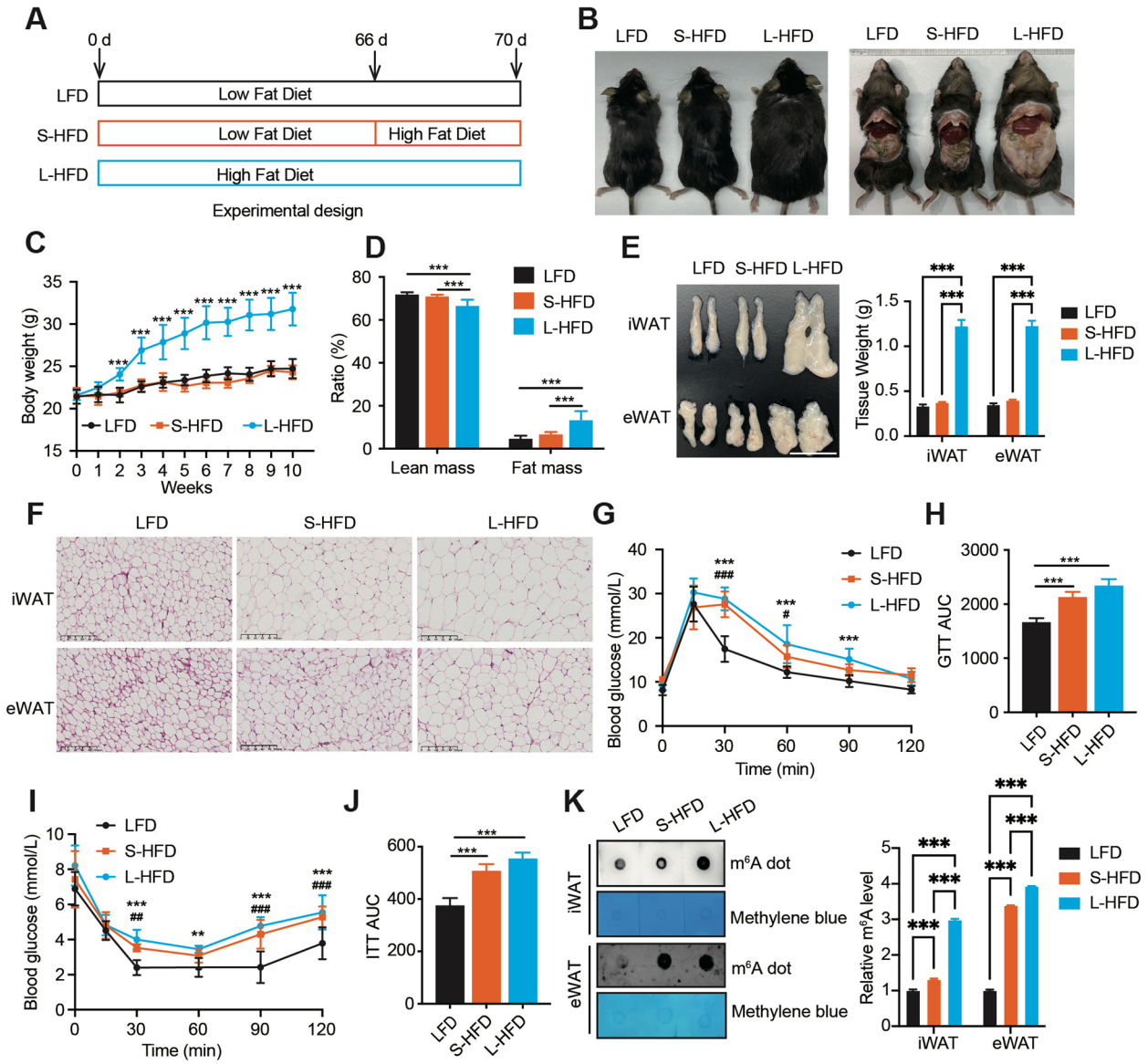

Fig. 1 Both short-term and long-term high fat diet feeding induce metabolic disorder and elevate m^{6}A level in WAT. **A** Mice were divided into three groups. Low fat diet (LFD): mice fed low fat diet for 10 weeks. Short-term high fat diet (S-HFD): mice fed low fat diet for 66 days, then fed high fat diet for 4 days. Long-term high fat diet (L-HFD): mice fed high fat diet for 10 weeks. **B** Representative photographs of mice in LFD, S-HFD and L-HFD group. **C** The growth curve of mice in LFD ($n=11$), S-HFD ($n=11$), and L-HFD group ($n=12$). One-way ANOVA for multiple comparisons were used for statistical analysis. $^*P<0.05$, $^{**}P<0.01$, $^{***}P<0.001$. **D** The ratio of lean mass and fat mass in mice from LFD ($n=10$), S-HFD ($n=10$), and L-HFD group ($n=12$). One-way ANOVA for multiple comparisons were used for statistical analysis. $^*P<0.05$, $^{**}P<0.01$, $^{***}P<0.001$. **E** Weight of iWAT and eWAT from LFD, S-HFD, and L-HFD group. One-way ANOVA for multiple comparisons were used for statistical analysis. $^*P<0.05$, $^{**}P<0.01$, $^{***}P<0.001$. **F** H&E staining of iWAT and eWAT from LFD, S-HFD, and L-HFD group. Scale bars, 100 μm. **G** Blood glucose levels of mice in LFD ($n=7$), S-HFD ($n=7$), and L-HFD ($n=8$) group during an intraperitoneal injection glucose tolerance test (GTT). $^{\#}P<0.05$, $^{\#\#}P<0.01$, and $^{\#\#\#}P<0.001$ were used to compare S-HFD and LFD. $^*P<0.05$, $^{**}P<0.01$, and $^{***}P<0.001$ were used to compare L-HFD and LFD. **H** The area under the curve (AUC) was calculated based on GTT results. One-way ANOVA for multiple comparisons was used for statistical analysis. $^*P<0.05$, $^{**}P<0.01$, $^{***}P<0.001$. **I** Blood glucose levels of mice in LFD ($n=8$), S-HFD ($n=8$), and L-HFD ($n=12$) group during an insulin tolerance test (ITT). $^{\#}P<0.05$, $^{\#\#}P<0.01$, and $^{\#\#\#}P<0.001$ were used to compare S-HFD and LFD. $^*P<0.05$, $^{**}P<0.01$, and $^{***}P<0.001$ were used to compare L-HFD and LFD. **J** The AUC was calculated based on ITT results. One-way ANOVA for multiple comparisons was used for statistical analysis. $^*P<0.05$, $^{**}P<0.01$, $^{***}P<0.001$. **K** mRNA m^{6}A modification level of iWAT and eWAT from LFD, S-HFD, and L-HFD mice were detected by dot-blot. Methylene blue staining was used as a loading control. The quantitative data of dot-blot results was calculated by Image **J**

height and weight, and strong evidence to total cholesterol and PC3 dietary pattern (Fig. 2K), indicating that increased ERVs may contribute to metabolic disorder by interacting with TFs, such as EP300. In contrast, MAFK showed very strong evidence to serum albumin and moderate evidence to adiponectin, fasting insulin, γ-glutamyl transferase, and height (Fig. 2L). Previous studies reported that serum albumin plays a role in estimating inflammatory activity [37], and adiponectin was correlated to obesity and insulin resistance [38], suggesting that increased LINEs may contribute to inflammation and insulin resistance during obesity by interacting with TFs, such as MAFK. Together, these results suggested that S-HFD and L-HFD respectively induced ERVs and LINEs which may contribute to different signaling pathway leading to metabolism disorder.

HFD-induced m^{6}A level increase of *Ehmt2* is responsible for activation of TEs and impaired metabolism.

Recent studies suggested that m^{6}A modifications on TE RNAs can regulate their stability and transcription [17]. Since mRNA m^{6}A level in eWAT was increased upon S-HFD and L-HFD feeding (Fig. 1K), thus we guessed that m^{6}A modification may participate in ERV or LINE regulation. To gain the transcriptome-wide m^{6}A profiling of eWAT, m^{6}A-seq of eWAT from LFD, S-HFD, and L-HFD groups were performed. Distribution analysis of m^{6}A peaks at distinct region (5′ untranslated region, 5′UTR; coding sequences, CDS; 3′ untranslated region, 3′UTR) showed that the majority of m^{6}A peaks was found in CDS region (Fig. 3A), and m^{6}A peaks were especially abundant in the vicinity of start and stop codons (Fig. 3B). The most enriched consensus motif identified from m^{6}A peaks was GGACU (Fig. 3C), which was conserved in the published consensus motif RRACH (where R = A/G, A = m^{6}A, and H = A/C/G) [17, 18]. To test whether m^{6}A regulated the TE expression, differential m^{6}A peaks were annotated to TEs. However, the RNA abundance of most TEs with differential m^{6}A level in S-HFD and L-HFD group was not differentially expressed when compared with LFD group (Fig. 3D, E). Consistently, there seems not obviously correlation between mRNA abundance and mRNA m^{6}A level (Fig. 3F, G). These results suggested that m^{6}A modification may not directly regulate TE activation in eWAT upon HFD feeding.

Notably, principal component analysis (PCA) of m^{6}A level of m^{6}A peaks showed that S-HFD and L-HFD induced more similar m^{6}A profile compared with LFD (Fig. 3H), which was consistent with the observed higher m^{6}A level upon HFD feeding by dot-blot (Fig. 1K). Furthermore, a cluster of genes with higher m^{6}A level both in S-HFD and L-HFD compared with LFD were identified (Fig. 3I), and these genes were significantly enriched in mRNA processing and covalent chromatin modification (Fig. 3J), in which chromatin modification, such as histone modification, was reported important for silencing TE expression [39, 40]. To identify whether there is a differential m^{6}A-modified gene which could regulate the expression of TEs through chromatin modification, genes with increased m^{6}A level upon HFD feeding and genes associated with covalent chromatin modification were overlayed, and *Ehmt2*, *Kat2b*, *Cdh5*, and *Huwe1* with higher m^{6}A level both in S-HFD and L-HFD group were screen out (Fig. 3K). It was noting that *Ehmt2*, a gene encoding protein as a H3K9me2 methyltransferase, was reported which could decrease the expression of ERVs [41] and LINE1 [42]. To determine the potential role of m^{6}A modification in *Ehmt2*, IGV viewer was subsequently employed to check the m^{6}A modification in *Ehmt2*. The results showed that the m^{6}A modification level in CDS region of *Ehmt2* in eWAT was much higher in S-HFD and L-HFD group compared to LFD group (Fig. 3L). MeRIP-qPCR results further demonstrated that the m^{6}A level of *Ehmt2* was significantly increased both in S-HFD and L-HFD group (Fig. 3M). Although the mRNA expression of *Ehmt2* was not changed (Fig. 3N), EHMT2 protein expression were remarkably decreased regardless of S-HFD and L-HFD (Fig. 3O). In line with the decreased EHMT2 expression, H3K9me2 level in eWAT was significantly decreased upon S-HFD and L-HFD feeding when compared with LFD feeding (Fig. 3O). To illustrate the role of EHMT2 on metabolism regulation, huge score of EHMT2 was calculated in T2DKP website.

(See figure on next page.)

Fig. 2 Activation of TEs is related to metabolic disorder phenotypes upon short-term and long-term HFD feeding. **A** GO enrichment results of up regulated genes in S-HFD compared with LFD. **B** GO enrichment results of upregulated genes in L-HFD compared with LFD. **C** GO enrichment results of upregulated genes in L-HFD compared with S-HFD. **D** GO enrichment results of downregulated genes in S-HFD compared with LFD. **E** GO enrichment results of downregulated genes in L-HFD compared with LFD. **F** GO enrichment results of downregulated genes in L-HFD compared with S-HFD. **G** Differential TEs in eWAT between S-HFD and LFD. **H** Differential TEs in eWAT between L-HFD and LFD. **I** Number and ratio plot of differential TEs in eWAT from L-HFD and SHFD compared to LFD. **J** Transcription factors significantly associated with the TEs of interest. The associations were analyzed by RTFAdb database. **K** HuGE Score of EP300 in the T2D-related diseases and traits. HuGE Score < 1 indicates no evidence, ≥ 3 indicates moderate evidence, ≥ 10 indicates strong evidence, and ≥ 30 indicates very strong evidence. **L** HuGE Score of MAFK in the T2D-related diseases and traits. HuGE Score < 1 indicates no evidence, ≥ 3 indicates moderate evidence, ≥ 10 indicates strong evidence, and ≥ 30 indicates very strong evidence

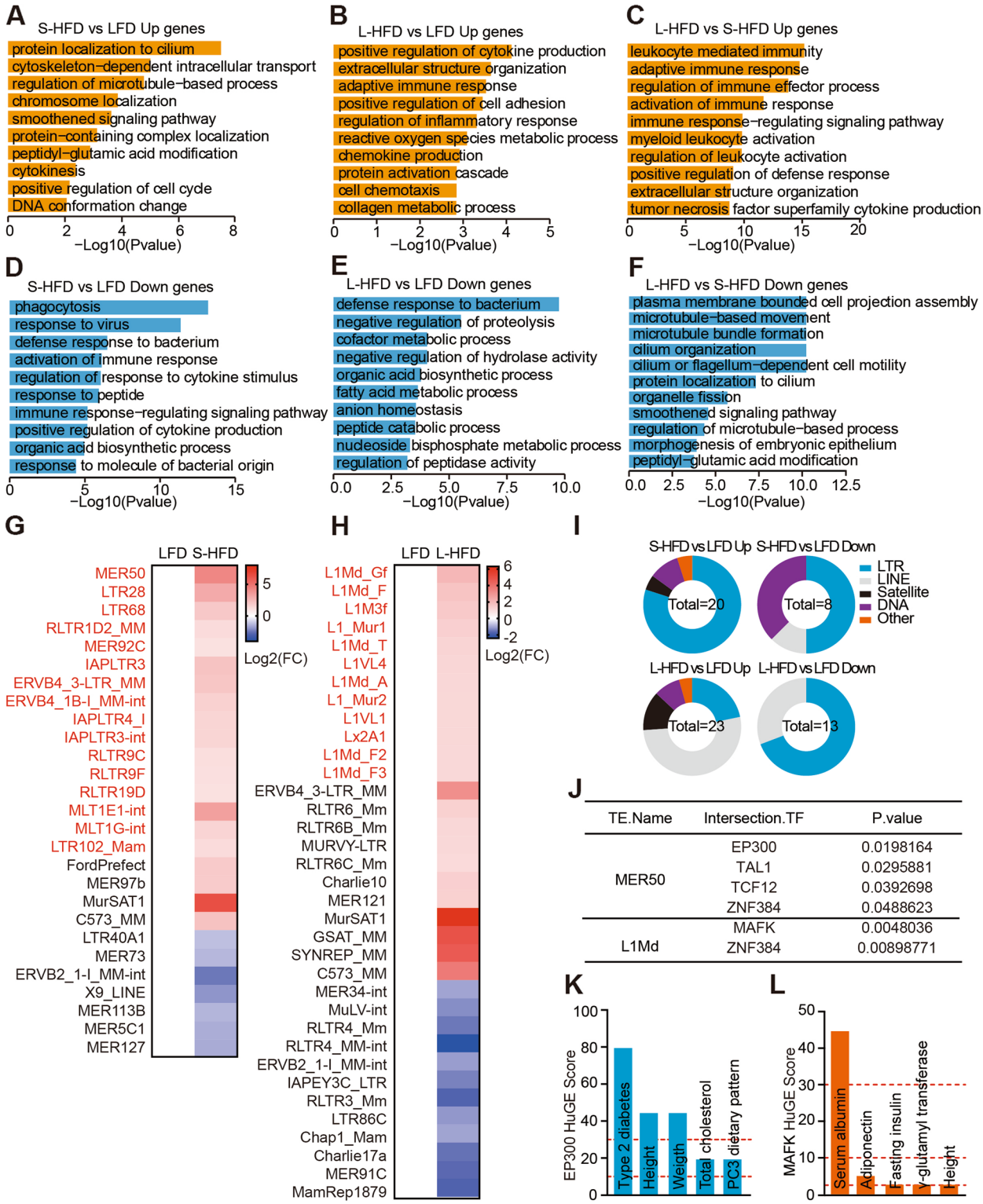

Fig. 2 (See legend on previous page.)

The results suggested that EHMT2 showed strong evidence to total cholesterol, waist-hip ratio, HbA1c, and T2D and moderate evidence to obesity (Fig. 3P), indicating a potential role of EHMT2 on metabolism regulation. To explore the role of EHMT2 in eWAT, EHMT2 plasmid was transfected into eWAT of mice in vivo, and mice were fed normal chow diet (NCD). Western blot results suggested that EHMT2 was successfully overexpressed in eWAT (Fig. 3Q). The results of GTT and ITT assays showed that overexpression of EHMT2 in eWAT could alleviate glucose intolerance and insulin insensitivity upon S-HFD feeding (Fig. 3R–U).

Previous studies demonstrated that antivirus medicine, such as Emtricitabine, could inhibit the expression of ERVs [14] and LINEs [43]. To illustrate whether the increased ERVs or LINEs was the reason of impaired metabolic health upon S-HFD and L-HFD feeding, antivirus treatment of mice was performed. The results showed that inhibited ERVs or LINEs could improve the glucose tolerance and insulin sensitivity under S-HFD feeding (Fig. 3R–U). Together, these results revealed that S-HFD and L-HFD feeding increased the m^{6}A level of *Ehmt2* and decreased the EHMT2 protein expression and H3K9me2 level, thereby activating ERVs and LINEs, resulting in metabolic disorder.

Gut microbiota is responsible for increased m^{6}A level in eWAT and metabolism disorder

Recently, numerous studies demonstrated that gut microbiota are involved in diet-induced obesity and metabolism disorder. To explore whether gut microbiota would play a role in S-HFD- and L-HFD-induced metabolism disorder, 16S rDNA sequencing of fecal samples from LFD and S-HFD and L-HFD group were performed (Figs. S2A and S2B, Tables S1 and S2). The principal coordinate analysis (PcoA) on family level of gut microbiota revealed a distinctly difference among LFD, S-HFD, and L-HFD fed mice (Fig. 4A). S-HFD and L-HFD changed the microbial composition on phylum level (Fig. 4B), especially increased Fimicutes/Bacteroidota (F/B) ratio (Fig. 4C), a potential marker indicating metabolism disorder in individuals and mice [44]. Besides, both S-HFD and L-HFD decreased the gut microbiome health index compared with LFD (Fig. 4D, E). To explore the differential gut microbiota, linear discriminant analysis (LDA) of gut microbiota was performed. Compared with LFD, S-HFD increased the abundance of uncultured_bacterium_g__norank_f__Desulfovibrionaceae and unclassified_f__Lachnospiraceae (Fig. 4F), while L-HFD increased abundance of Lachnospiraceae_bacterium_28-4 and Romboutsia_ilealis (Fig. 4G). These results suggested that both S-HFD and L-HFD disrupted the gut microbiota composition.

Since numerous studies demonstrated that gut microbiota could regulate the m^{6}A modification in specific tissues [45, 46]. To study whether gut microbiota could affect the mRNA m^{6}A modification in eWAT and impaired metabolism health, fecal microbiota from LFD, S-HFD, and L-HFD group were transplanted into antibiotic-treated (Abx) mice, and all mice were fed with NCD. Compared with LFD fed mice fecal microbiota recipient mice (Fig. S2C), mice received fecal microbiota from S-HFD and L-HFD increased the size of iWAT and eWAT (Fig. 4H), tissue weight, and adipocyte size in eWAT (Fig. 4I–K). More importantly, transplantation of fecal microbiota from S-HFD and L-HFD increased m^{6}A level in eWAT (Fig. 4L), as well as induced glucose intolerance and insulin insensitivity (Fig. 4M–P). These results

(See figure on next page.)

Fig. 3 HFD-induced m^{6}A level increase of *Ehmt2* is responsible for activation of TEs and impaired metabolism. **A** Transcriptome-wide distribution of mRNA m^{6}A peak. The bar chart shows the percentages of m^{6}A peak within distinct regions: CDS, 5'UTR, and 3'UTR. **B** The m^{6}A peak distribution pattern within mRNA in different regions: 5'UTR, CDS, and 3'UTR. **C** The most enriched consensus motif identified from m^{6}A peaks on exons by HOMER software. **D** Veen plot of differentially expressed TEs and differentially methylated TEs between S-HFD and LHFD. **E** Veen plot of differentially expressed TEs and differentially methylated TEs between L-HFD and LFD. **F** Four-quadrant plots to show the mRNAs with a significant change both in m^{6}A level and mRNA levels between S-HFD and LHFD. **G** Four-quadrant plots to show the mRNAs with a significant change both in m^{6}A level and mRNA levels between L-HFD and LFD. **H** PCA results of based on m^{6}A level in eWAT from LFD, S-HFD, and L-HFD group. **I** Unsupervised clustering analysis of m^{6}A level in eWAT from LFD, S-HFD, and L-HFD group. **J** GO enrichment results of genes with increased m^{6}A level in eWAT from S-HFD and L-HFD group compared to LFD group. **K** Veen plot of genes with increased m^{6}A level in S-HFD or L-HFD group and genes involving in covalent chromatin modification. **L** m^{6}A peak of *Ehmt2* in eWAT from LFD, S-HFD, and L-HFD group was visualized by integrative genomics viewer. **M** MeRIP-qPCR results of m.^{6}A level of *Ehmt2* mRNA in eWAT from LFD, S-HFD, and L-HFD group. **N** qPCR results of *Ehmt2* mRNA expression in eWAT from LFD, S-HFD, and L-HFD group. **O** Western blot results of EHMT2 protein expression and H3K9me2 level in eWAT from LFD, S-HFD, and L-HFD group. **P** HuGE Score of EHMT2 in the T2D-related diseases and traits. HuGE Score < 1 indicates no evidence, ≥ 3 indicates moderate evidence, ≥ 10 indicates strong evidence, and ≥ 30 indicates very strong evidence. **Q** Western blot results of EHMT2 protein expression in eWAT transfected with or without EHMT2 plasmid. **R** Blood glucose levels of mice in NCD ($n = 6$), S-HFD ($n = 6$), S-HFD + OE-EHMT2 ($n = 6$), and S-HFD + antivirus ($n = 6$) groups during GTT assay. **S** AUC was calculated based on GTT results. One-way ANOVA for multiple comparisons was used for statistical analysis. *$P < 0.05$, **$P < 0.01$, ***$P < 0.001$. **T** Blood glucose levels of mice in NCD ($n = 6$), S-HFD ($n = 6$), S-HFD + OE-EHMT2 ($n = 6$), and S-HFD + antivirus ($n = 6$) groups during ITT assay. **U** The AUC was calculated based on ITT results. One-way ANOVA for multiple comparisons was used for statistical analysis. *$P < 0.05$, **$P < 0.01$, ***$P < 0.001$

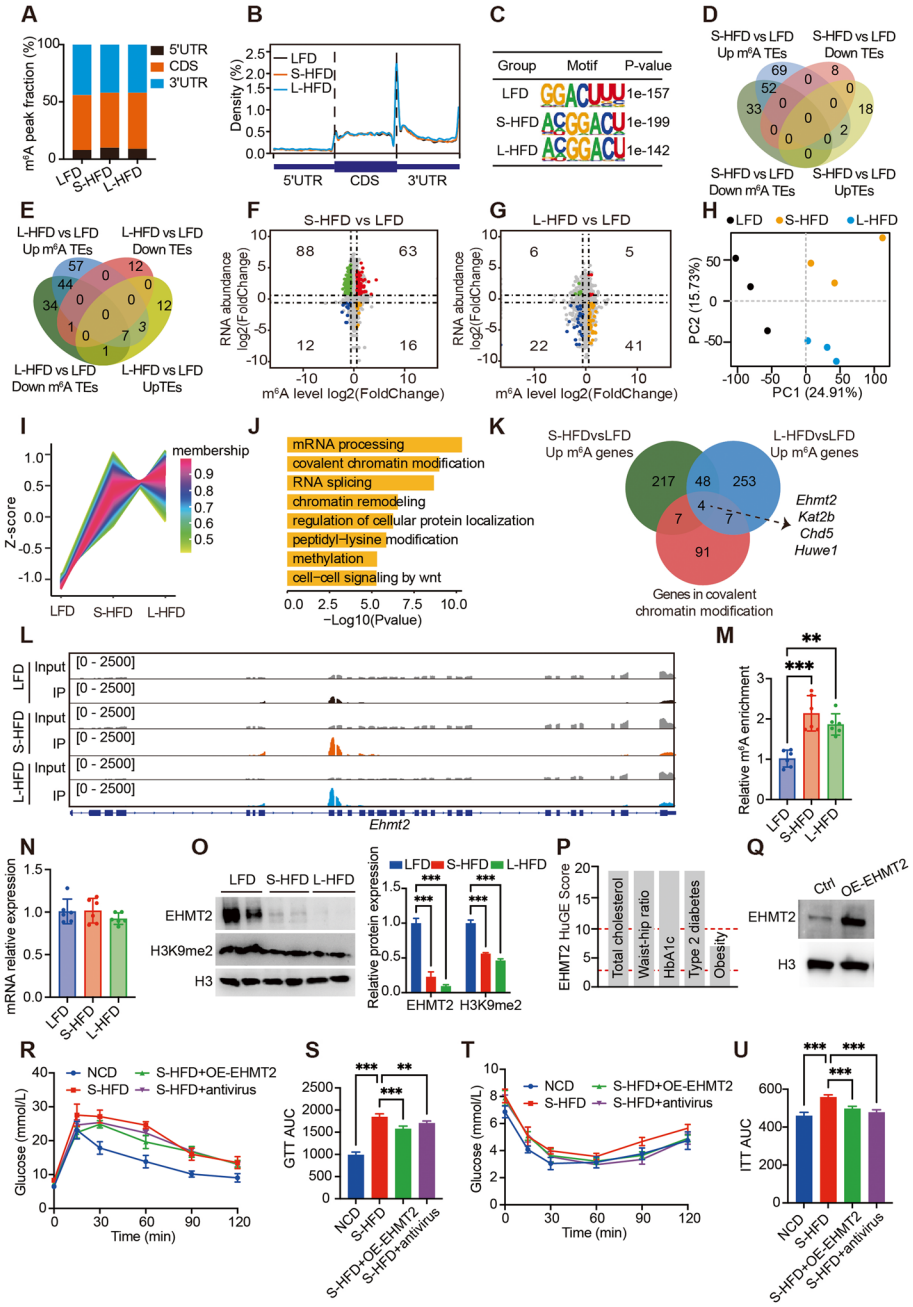

Fig. 3 (See legend on previous page.)

suggested that S-HFD and L-HFD increased m^{6}A level in eWAT and impaired metabolism health by disrupting gut microbiota.

Gut microbiota-derived homogentisic increased m^{6}A level in eWAT and impaired metabolism

Generally, the gut microbiota produces a myriad of metabolites that affect host physiology and metabolic health [47]. To identify potential gut microbial metabolites which could regulate m^{6}A, untargeted metabolomics analyses of fecal samples from LFD, S-HFD, and L-HFD fed mice were performed. The results of partial least square discriminant analysis (PLS-DA) showed that metabolites were distinctly divided into LFD, S-HFD, and L-HFD group, in which metabolites from S-HFD and L-HFD clustered more closer (Fig. 5A). To gain the key metabolites in each group, metabolite variable importance in the projection value (VIP)

analysis was performed, and top 30 differential metabolites were identified (Figs. S3A and S3B). To screen out potential metabolites related to metabolism disorder, the top 30 differential metabolites in this study were overlapped with previously reported obesity and T2D-related metabolites [48]. Interestingly, only homogentisic acid (HGA) was identified (Fig. 5B), and the abundance of HGA was much higher both in S-HFD and L-HFD group compared to LFD group (Fig. 5C). Consistently, the results of HGA concentration in feces showed that HGA was increased both in S-HFD and L-HFD compared to LFD (Fig. S3C). To explore which gut microbiota was responsible for HGA production, correlation analysis between gut microbiota abundance and HGA level was performed. The results showed that HGA level was positively correlated with unclassified_f__Lachnospiraceae which was increased in S-HFD and L-HFD feeding mice. Besides, Lachnospiraceae_bacterium_28-4 and Romboutsia_ilealis from L-HFD feeding mice were positively correlated with HGA level, and uncultured_bacterium_g__Dubosiella from LFD feeding mice was negatively correlated with HGA level (Fig. 5D).

To determine whether HGA plays a role in m^{6}A regulation, 8-week-old male mice were injected intraperitoneally with 250 mg/kg HGA daily for 4 days as previously reported [16, 49, 50], and mice were fed with NCD. eWAT was isolated to analyze m^{6}A level, and the results showed that HGA treatment increased the overall mRNA m^{6}A level in eWAT (Fig. 5E) and the m^{6}A level of *Ehmt2* mRNA (Fig. 5F). Although HGA treatment did not affect the mRNA expression of *Ehmt2* (Fig. 5G), HGA treatment increased the protein expression of EHMT2 and H3K9me2 level in eWAT (Fig. 5H), which was consistent with the results observed in eWAT from LFD, S-HFD, and L-HFD group (Fig. 3M–O). To validate the role of HGA on metabolism health, GTT and ITT assays were performed after 4 days HGA treatment. The results showed that HGA treatment significantly impaired glucose tolerance and insulin sensitivity (Fig. 5I–L). Taken together, these findings suggested that HGA served as the potential metabolite responsible for HFD-induced m^{6}A level increase and EHMT2 expression decrease, leading to metabolism disorder regardless of S-HFD and L-HFD feeding (Fig. 5M).

Discussion

It has been demonstrated that acute lipid overload for 5 h or short-term (3–7 days) HFD intake results in impaired glucose uptake of adipose tissue and systemic insulin resistance [4, 5, 51]. The systemic insulin resistance steadily worsened with increasing adipose tissue inflammation and obesity upon L-HFD intake [52]. Nonetheless, our knowledge of the underlying mechanism of S-HFD- and L-HFD-induced metabolism disorder is still limited. Here, we demonstrated that both 4 days S-HFD and 10 weeks L-HFD feeding significantly impaired whole body glucose tolerance and insulin sensitivity. Moreover, we found that both S-HFD and L-HFD increased the m^{6}A level in WAT, especially in eWAT. It has been reported that 3 weeks of mouse maternal HFD intake increased mRNA m^{6}A modifications in eWAT in offspring, but 8 or 15 weeks of mouse maternal HFD intake showed opposite results [11]. Previous study suggested that the administration of curcumin significantly increased m^{6}A level in iWAT and prevents HFD-induced obesity [13]. Thus, the alteration of m^{6}A level in eWAT upon S-HFD and L-HFD feeding suggested a potential role of m^{6}A on HFD-induced metabolism disorder.

Previous study suggested that the initial stage of HFD-induced insulin resistance is independent of inflammation, whereas the more chronic state of insulin resistance in established obesity is largely mediated by proinflammatory actions [4]. Ji et al. reported that S-HFD feeding induced remarkably pronounced immune responses and inflammation in eWAT, which may account for impaired metabolic health [53]. In this regard, our finding revealed

(See figure on next page.)

Fig. 4 Gut microbiota is responsible for increased m^{6}A level in eWAT and metabolism disorder. **A** PcoA plot on family level of 16S rDNA data from LFD ($n=9$), S-HFD ($n=9$), and L-HFD ($n=10$) groups. **B** Phylum level taxonomy and relative abundance in 16S rDNA data from LFD, S-HFD, and L-HFD groups. **C** Fimicutes/Bacteroidota ratio in LFD, S-HFD, and L-HFD groups. **D** Gut microbiome health index between LFD and S-HFD groups. **E** Gut microbiome health index between LFD and L-HFD groups. **F** LDA scores of gut microbiota at species level in LFD and S-HFD groups. **G** LDA scores of gut microbiota at species level in LFD and L-HFD groups. **H** Representative photographs of iWAT and eWAT in Abx-LFD, Abx-S-HFD, and Abx-L-HFD groups. **I** Tissue weight of eWAT from Abx-LFD, Abx-S-HFD, and Abx-L-HFD groups. One-way ANOVA for multiple comparisons was used for statistical analysis. *$P<0.05$, **$P<0.01$, ***$P<0.001$. **J** H&E staining of eWAT in Abx-LFD, Abx-S-HFD, and Abx-L-HFD groups. Scale bars, 20 μm. **K** Mean adipocyte size of eWAT from Abx-LFD, Abx-S-HFD, and Abx-L-HFD groups. One-way ANOVA for multiple comparisons was used for statistical analysis. *$P<0.05$, **$P<0.01$, ***$P<0.001$. **L** Dot-blot analysis of mRNA m.^{6}A level in eWAT from Abx-LFD, Abx-S-HFD, and Abx-L-HFD groups. Methylene blue staining was used as a loading control. The quantitative data of dot-blot results was calculated by Image J. **M** Blood glucose levels of mice in Abx-LFD ($n=5$), Abx-S-HFD ($n=6$), and Abx-L-HFD ($n=6$) groups during GTT assay. **N** The AUC was calculated based on GTT results. One-way ANOVA for multiple comparisons was used for statistical analysis. *$P<0.05$, **$P<0.01$, ***$P<0.001$. **O** Blood glucose levels of mice in Abx-LFD ($n=5$), Abx-S-HFD ($n=6$), and Abx-L-HFD ($n=6$) groups during ITT assay. **P** The AUC was calculated based on ITT results. One-way ANOVA for multiple comparisons was used for statistical analysis. *$P<0.05$, **$P<0.01$, ***$P<0.001$

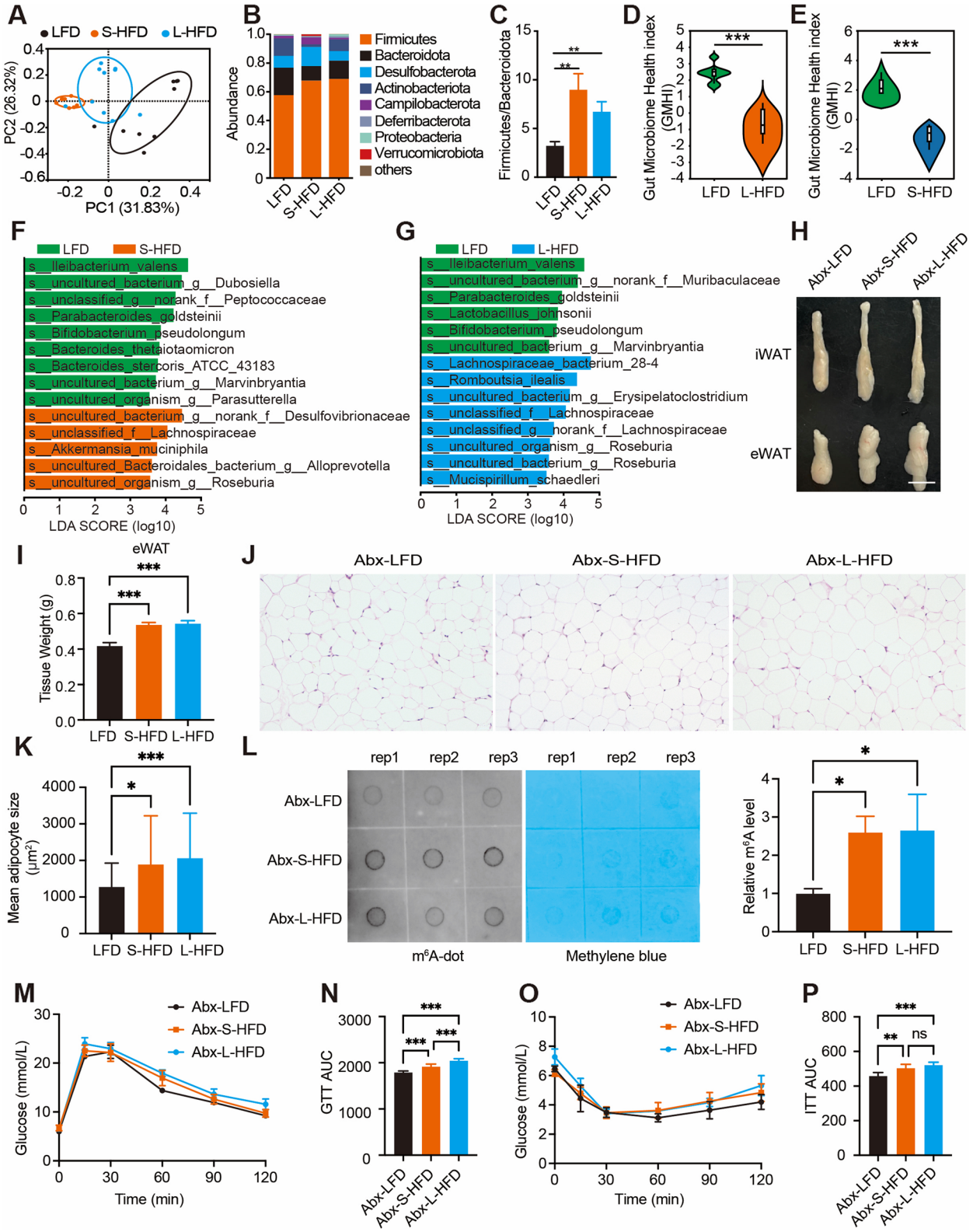

Fig. 4 (See legend on previous page.)

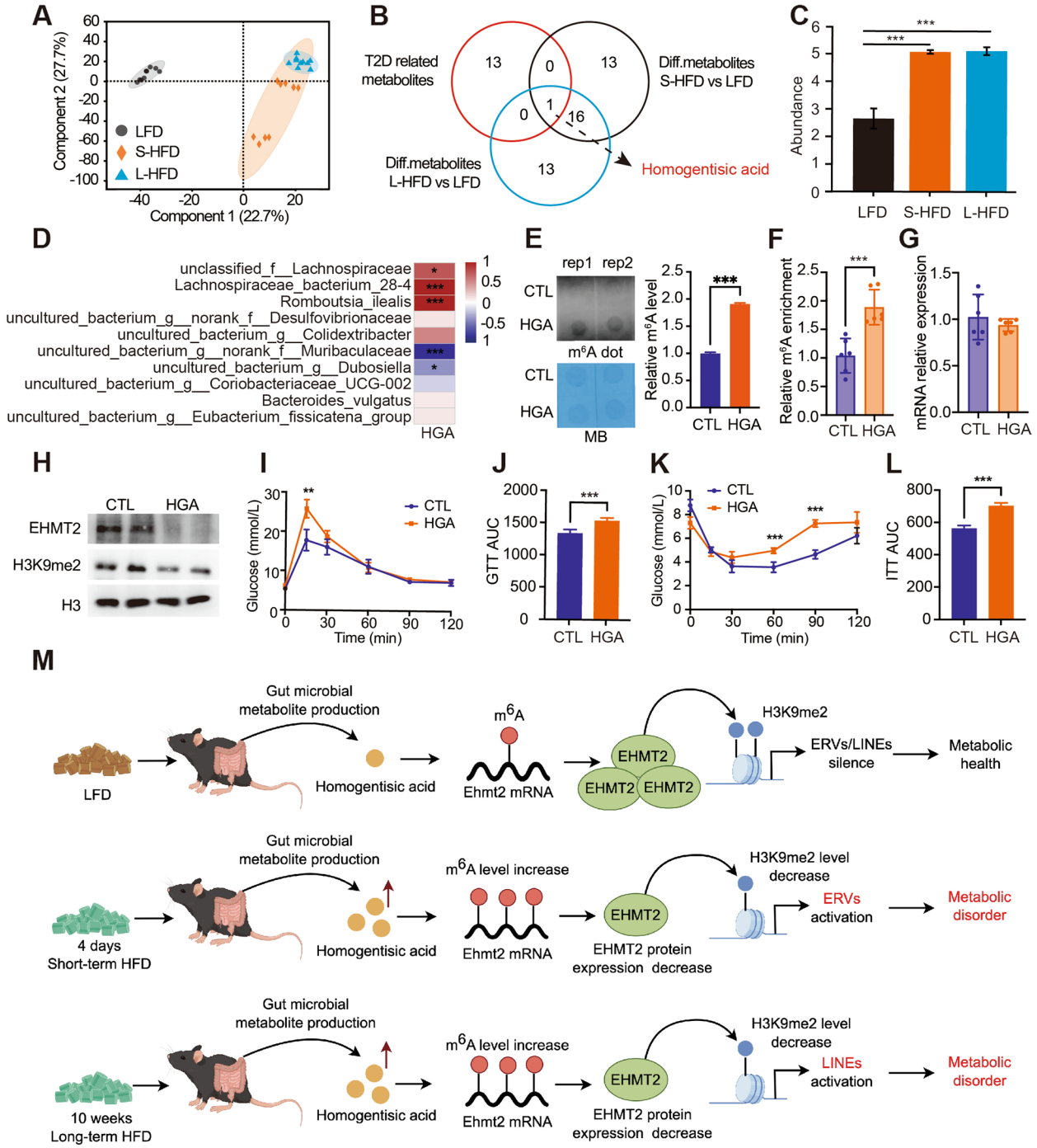

Fig. 5 Gut microbiota-derived homogentisic increased m^{6}A level in eWAT and impaired metabolism. **A** PLS-DA for gut metabolites in LFD ($n=9$), S-HFD ($n=9$), and L-HFD ($n=10$) group. **B** Overlap results between T2D-related metabolites and differential metabolites from S-HFD and L-HFD compared to LFD. **C** Abundance of HGA based on untargeted metabolomics results from LFD, S-HFD, and L-HFD groups. One-way ANOVA for multiple comparisons was used for statistical analysis. *$P<0.05$, **$P<0.01$, ***$P<0.001$. **D** Heatmap plot of Spearman correlation results between gut microbiotas and HGA. **E** Dot-blot analysis of mRNA m^{6}A level in eWAT from mice treated with or without HGA. Methylene blue staining was used as a loading control. **F** MeRIP-qPCR results of m.^{6}A level of *Ehmt2* mRNA in eWAT from mice treated with or without HGA. **G** qPCR results of *Ehmt2* mRNA expression in eWAT from mice treated with or without HGA. **H** Western blot results of EHMT2 and H3K9me2 expression in eWAT from mice treated with or without HGA. **I** GTT results of 8-week-old mice treated with or without HGA for 3 days ($n=5$ per group). **J** The AUC was calculated based on GTT results. Student's *t*-test was used for statistical analysis. *$P<0.05$, **$P<0.01$, ***$P<0.001$. **K** ITT results of 8-week-old mice treat with or without HGA ($n=5$ per group). **L** The AUC was calculated based on ITT results. Student's *t*-test was used for statistical analysis. *$P<0.05$, **$P<0.01$, ***$P<0.001$

that S-HFD did not induce obvious proinflammatory at transcript level, but increase nutrition sensing ability of adipose tissue by promoting cilium-related function and cell cycle. S-HFD was reported to promote proliferation capacity of preadipocyte and adipose tissue hyperplasia [54]. As for L-HFD, a proinflammatory response was found in eWAT at transcript level, which was consistent with previous studies [55, 56]. To our surprise, a function of response to virus was found in eWAT after S-HFD feeding, which was not reported before. Recently, HFD was reported to promote ERV expression involving in response to virus in keratinocytes [14]. Here, we revealed that S-HFD-induced expression of ERVs, whereas L-HFD activated expression of LINEs. In fact, numerous studies suggested that retrotransposons contained cis-regulatory sequences binding to TFs to regulate gene expression in diseases and tissue development [57]. Fresquet et al. found that epigenetic therapy killed cancer cells by rewiring mitochondrial metabolism upon ERV activation [58]. Another study reported that specific ERV function as active enhancers to drive germline genes during mitosis-to-meiosis transition in male mice [59]. Hansen et al. revealed that several waist-to-hip ratio-associated variants map within primate-specific Alu retrotransposons harboring a DNA motif associated with adipocyte differentiation [60]. Our findings suggested that S-HFD-induced ERVs showing potential interaction with TFs, such as EP300 involving in T2D disease. EP300 functions as histone acetyltransferase that regulates transcription via chromatin remodeling and is important in various biological processes. EP300-mediated acetylation of histones alters global chromatin structure and gene expression, promoting the development and progression of fibrosis [61]. Additionally, knockdown of EP300 in human aortic endothelial cells suppressed diabetes-related genes including CD58, SIGIRR, CD200, ICAM2, and CCL2 [62]. However, L-HFD induced LINEs showing potential association with TFs, such as MAFK which was related to inflammation. It was known that MafK positively regulates NF-κB activity by enhancing CBP-mediated p65 acetylation facilitating recruitment of p65 to NF-κB promoters such as IL-8 and TNFα [63]. Thus, EP300 and MAFK may promote the expression of obesity-related genes to induce metabolic disorder through transcriptional regulation. These results indicated that activation of specific TEs may play an important role in metabolism upon HFD feeding.

Generally, TEs were silenced by deposit of DNA and histone modification, such as DNA methylation and H3K9me2, at TEs loci, which was mediated by TE regulators [59]. In this study, we found that both S-HFD and L-HFD feeding could significantly increase m^6A level of *Ehmt2* mRNA and decrease EHMT2 protein expression as well as H3K9me2 level in eWAT. It has been reported that EHMT2, the H3K9me2 methyltransferase, suppressed both ERVs [41] and LINE1 elements [42]. Thus, the specific TE expression in this study may activate by the removal of H3K9me2 mediated by downregulated EHMT2 expression. Other studies reported that EHMT2 was markedly decreased in the liver of db/db mice and HFD-fed mice, thereby impairing hepatic insulin signaling [64]. Hepatic *Ehmt2* knockdown exacerbated Dex-induced glucose and insulin intolerance [65]. Muscle-specific KO of *Ehmt2* protected against obesity under HFD stress in female but not in male mice [66]. Removal of H3K9me2 in adipocytes by EHMT2 deletion enhanced chromatin opening and binding of the early adipogenic transcription factor Cebpb to Pparg promoter, thus promoting adipogenesis [67]. Loss of EHMT2 in adipocytes exacerbated TNFα's deleterious effects on inflammatory gene expression and lipolysis [68]. In immune cells, such as macrophages, EHMT2-dependent H3K9me2 was associated with gene repression during endotoxin tolerance [69], suggesting that EHMT2 plays a critical role in immune cell function. More in-depth research about the specific role of EHMT2 in adipocytes and immunes will be helpful to understand the underlying mechanism contributing metabolic disorder upon HFD feeding. Nonetheless, our results suggested that overexpression of EHMT2 in eWAT could alleviate HFD-induced metabolism disorder. Together, these results provided a potential evidence linking dietary fat, metabolism, and TEs, where HFD-induced m^6A reprogramming modulate the TEs activation by EHMT2 resulting in metabolic disorder.

Recently, more and more studies demonstrated that HFD-feeding induces obesity and the epigenetic modification of host tissues by altering gut microbiota. Wang et al. found transcriptome-wide reprogramming of mRNA m^6A modification by the mouse microbiome [45]. Another study showed the impact of the gut microbiota on the mRNA m^6A of mouse cecum and liver [46]. In this study, we found that both S-HFD and L-HFD could significantly shape the gut microbiota composition and increase F/B ratio which was previously reported serve as a biomarker of obesity and metabolic disorder [44]. Furthermore, we identified HGA, a gut microbial metabolite which was significantly increased both in S-HFD and L-HFD group, was responsible for increased mRNA m^6A level of *Ehmt2* and decreased EHMT2 expression as well as H3K9me2 level, leading to impaired metabolic health. However, the underlying mechanism of HGA on m^6A level regulation is unclear. It has been demonstrated that HGA could be transformed to the TCA cycle intermediates such as fumaric acid and succinic acid [70] which

was reported to inhibit m^{6}A demethylase including ALKBH5 and FTO, providing a potential mechanism of HGA on m^{6}A regulation [71]. In human, the expression of m^{6}A regulators correlated with human obesity [72]. TEs, such as LINE-1, in human visceral adipose tissue is associated with metabolic syndrome status and related phenotypes [73]. Besides, HGA showed the strongest positive associations with body mass index, waist circumference, and increased T2D risk [74]. Despite the advancement we found in mice, more in-depth research in human samples needs to be conduct to study the integrated mechanisms about diet, m^{6}A, gut microbiome in regulating human metabolic health.

Conclusions

In summary, we demonstrated that both short-term and long-term HFD feeding increased m^{6}A level in WAT and systemic metabolic disorder. Moreover, we provided an evidence that HFD increased m^{6}A level of *Ehmt2*, thereby downregulated EHMT2 expression and H3K9me2 level, and activated TE expression, resulting in metabolic disorder. Finally, we found that gut-microbiota derived HGA serve as the key factor for HFD-induced m^{6}A epitranscriptome reprogramming and impaired metabolic health. Our findings provided a novel mechanism and function of m^{6}A-mediated TE activation in metabolic disorder, highlighting the interaction role of host mRNA modification and gut microbiota on metabolic health regulation.

Abbreviations

Abx	Antibiotic treated
CDS	Coding sequences
EHMT2	Euchromatic histone lysine methyltransferase 2
ERVs	Endogenous retroviruses
eWAT	Epididymal white adipose tissue
GO	Gene ontology
GTT	Glucose tolerance test
HFD	High-fat diet
HGA	Homogentisic acid
HuGE	Human genetic evidence
ITT	Insulin tolerance test
iWAT	Inguinal white adipose tissue
LEfSe	Linear discriminant analysis effect size
LFD	Low-fat diet
L-HFD	Long-term HFD
LINEs	Long interspersed elements
m^{6}A-seq	M^{6}A sequencing
PCA	Principal component analysis
PcoA	Principal coordinate analysis
PLS-DA	Partial least squares discriminant analysis
qPCR	Quantitative real-time PCR
RNA-seq	RNA sequencing
S-HFD	Short-term HFD
T2D	Type 2 diabetes
T2DKP	T2D knowledge portal
TEs	Transposable elements
TFs	Transcription factors
UTR	Untranslated region

Supplementary Information

The online version contains supplementary material available at https://doi.org/10.1186/s40168-025-02047-4.

Supplementary Material 1.
Supplementary Material 2.
Supplementary Material 3.
Supplementary Material 4.
Supplementary Material 5.

Acknowledgements

Not applicable.

Authors' contributions

LYH., LJQ., RRT., XZM., LYJ., CYS., HCQ., LYX. and YTYD. performed experiments under the supervision of WXX. LYH. and LJQ. performed bioinformatics analysis of sequence data. LYH. wrote the manuscript under the supervision of WXX. WXX. designed the project and provided the final approval of the manuscript.

Funding

This work was supported by the National Natural Science Foundation of China (32330098), the Science and Technology Innovation Leading Talent Project of Zhejiang Province (2022R52023), the National Natural Science Foundation of China (U21A20249), and the National Key R&D Program of China (2023YFD1301303).

Data availability

The m6A-seq datasets (CRA011918, https://ngdc.cncb.ac.cn/gsa/s/f0FDR4S1) have been deposited in the Genome Sequence Archive linked to the project PRJCA018477. The 16S rDNA datasets (CRA011935, https://ngdc.cncb.ac.cn/gsa/s/r0dY3Uu3) have been deposited in the Genome Sequence Archive linked to the project PRJCA018487. Untargeted metabolomic datasets (OMIX004571, https://ngdc.cncb.ac.cn/omix/preview/ImckzEo4) have been deposited in OMIX linked to the project PRJCA018487.

Declarations

Ethics approval and consent to participate

All experimental procedures used in this study were approved by the Committee on Animal Care and Use and Committee on the Ethics of Animal Experiments of Zhejiang University.

Consent for publication

Not applicable.

Competing interests

The authors declare no competing interests.

Author details

[1]College of Animal Sciences, Zhejiang University, Hangzhou, Zhejiang, China. [2]Key Laboratory of Animal Nutrition and Feed Science (Eastern of China), Ministry of Agriculture and Rural Affairs, Hangzhou, China. [3]Laboratory of Molecular Animal Nutrition (Zhejiang University), Ministry of Education, Hangzhou, China. [4]Zhejiang Key Laboratory of nutrition and breeding for high-quality animal products, Hangzhou, Zhejiang, China.

Received: 13 June 2024 Accepted: 22 January 2025
Published online: 17 March 2025

References

1. Sárvári AK, Van Hauwaert EL, Markussen LK, Gammelmark E, Marcher A-B, Ebbesen MF, et al. Plasticity of epididymal adipose tissue in response to diet-induced obesity at single-nucleus resolution. Cell Metab. 2021;33:437-453.e5.

2. Nahmgoong H, Jeon YG, Park ES, Choi YH, Han SM, Park J, et al. Distinct properties of adipose stem cell subpopulations determine fat depot-specific characteristics. Cell Metab. 2022;34:458-472.e6.
3. Emont MP, Jacobs C, Essene AL, Pant D, Tenen D, Colleluori G, et al. A single-cell atlas of human and mouse white adipose tissue. Nature. 2022;603:926–33.
4. Lee YS, Li P, Huh JY, Hwang IJ, Lu M, Kim JI, et al. Inflammation is necessary for long-term but not short-term high-fat diet–induced insulin resistance. Diabetes. 2011;60:2474–83.
5. Paglialunga S, Ludzki A, Root-McCaig J, Holloway GP. In adipose tissue, increased mitochondrial emission of reactive oxygen species is important for short-term high-fat diet-induced insulin resistance in mice. Diabetologia. 2015;58:1071–80.
6. Foley KP, Zlitni S, Denou E, Duggan BM, Chan RW, Stearns JC, et al. Long term but not short term exposure to obesity related microbiota promotes host insulin resistance. Nat Commun. 2018;9:4681.
7. Ying W, Gao H, Dos Reis FCG, Bandyopadhyay G, Ofrecio JM, Luo Z, et al. MiR-690, an exosomal-derived miRNA from M2-polarized macrophages, improves insulin sensitivity in obese mice. Cell Metab. 2021;33:781-790.e5.
8. Sun W, von Meyenn F, Peleg-Raibstein D, Wolfrum C. Environmental and nutritional effects regulating adipose tissue function and metabolism across generations. Adv Sci (Weinh). 2019;6:1900275.
9. Wang X, Wu R, Liu Y, Zhao Y, Bi Z, Yao Y, et al. m ^{6} A mRNA methylation controls autophagy and adipogenesis by targeting *Atg5* and *Atg7*. Autophagy. 2020;16:1221–35.
10. Tao X, Du R, Guo S, Feng X, Yu T, OuYang Q, et al. PGE2 -EP3 axis promotes brown adipose tissue formation through stabilization of WTAP RNA methyltransferase. EMBO J. 2022;41:e110439.
11. Li X, Yang J, Zhu Y, Liu Y, Shi X, Yang G. Mouse maternal high-fat intake dynamically programmed mRNA m^{6}A modifications in adipose and skeletal muscle tissues in offspring. Int J Mol Sci. 2016;17:1336.
12. Wu R, Yao Y, Jiang Q, Cai M, Liu Q, Wang Y, et al. Epigallocatechin gallate targets FTO and inhibits adipogenesis in an mRNA m6A-YTHDF2-dependent manner. Int J Obes (Lond). 2018;42:1378–88.
13. Chen Y, Wu R, Chen W, Liu Y, Liao X, Zeng B, et al. Curcumin prevents obesity by targeting TRAF4-induced ubiquitylation in m6A-dependent manner. EMBO Rep. 2021;22:e52146.
14. Lima-Junior DS, Krishnamurthy SR, Bouladoux N, Collins N, Han S-J, Chen EY, et al. Endogenous retroviruses promote homeostatic and inflammatory responses to the microbiota. Cell. 2021;184:3794-3811.e19.
15. Xie J, Li H, Zhang X, Yang T, Yue M, Zhang Y, et al. Akkermansia muciniphila protects mice against an emerging tick-borne viral pathogen. Nat Microbiol. 2023;8:91–106.
16. Du Z, Su J, Lin S, Chen T, Gao W, Wang M, et al. Hydroxyphenylpyruvate dioxygenase is a metabolic immune checkpoint for UTX-deficient colorectal cancer. Gastroenterology. 2023;164:1165-1179.e13.
17. Liu J, Dou X, Chen C, Chen C, Liu C, Xu MM, et al. N6-methyladenosine of chromosome-associated regulatory RNA regulates chromatin state and transcription. Science. 2020;367:580–6.
18. Wei J, Yu X, Yang L, Liu X, Gao B, Huang B, et al. FTO mediates LINE1 m6A demethylation and chromatin regulation in mESCs and mouse development. Science. 2022;376:968–73.
19. Bolger AM, Lohse M, Usadel B. Trimmomatic: a flexible trimmer for Illumina sequence data. Bioinformatics. 2014;30:2114–20.
20. Dobin A, Davis CA, Schlesinger F, Drenkow J, Zaleski C, Jha S, et al. STAR: ultrafast universal RNA-seq aligner. Bioinformatics. 2013;29:15–21.
21. Zhang Y, Liu T, Meyer CA, Eeckhoute J, Johnson DS, Bernstein BE, et al. Model-based analysis of ChIP-Seq (MACS). Genome Biol. 2008;9:R137.
22. Liu L, Zhang S-W, Huang Y, Meng J. QNB: differential RNA methylation analysis for count-based small-sample sequencing data with a quad-negative binomial model. BMC Bioinformatics. 2017;18:387.
23. Heinz S, Benner C, Spann N, Bertolino E, Lin YC, Laslo P, et al. Simple combinations of lineage-determining transcription factors prime cis-regulatory elements required for macrophage and B cell identities. Mol Cell. 2010;38:576–89.
24. Wu T, Hu E, Xu S, Chen M, Guo P, Dai Z, et al. clusterProfiler 4.0: a universal enrichment tool for interpreting omics data. Innovation (Camb). 2021;2:100141.
25. Chen H, Zhao X, Yang W, Zhang Q, Hao R, Jiang S, et al. RNA N6-methyladenosine modification-based biomarkers for absorbed ionizing radiation dose estimation. Nat Commun. 2023;14:6912.
26. Liao Y, Smyth GK, Shi W. featureCounts: an efficient general purpose program for assigning sequence reads to genomic features. Bioinformatics. 2014;30:923–30.
27. Love MI, Huber W, Anders S. Moderated estimation of fold change and dispersion for RNA-seq data with DESeq2. Genome Biol. 2014;15:550.
28. Clapes T, Polyzou A, Prater P, Sagar null, Morales-Hernández A, Ferrarini MG, et al. Chemotherapy-induced transposable elements activate MDA5 to enhance haematopoietic regeneration. Nat Cell Biol. 2021;23:704–17.
29. Jin Y, Tam OH, Paniagua E, Hammell M. TEtranscripts: a package for including transposable elements in differential expression analysis of RNA-seq datasets. Bioinformatics. 2015;31:3593–9.
30. Edgar RC. UPARSE: highly accurate OTU sequences from microbial amplicon reads. Nat Methods. 2013;10:996–8.
31. Chappidi S, Villa EC, Cantarel BL. Using Mothur to determine bacterial community composition and structure in 16S ribosomal RNA datasets. Curr Protoc Bioinformatics. 2019;67:e83.
32. Gupta VK, Kim M, Bakshi U, Cunningham KY, Davis JM, Lazaridis KN, et al. A predictive index for health status using species-level gut microbiome profiling. Nat Commun. 2020;11:4635.
33. Wu R, Liu Y, Yao Y, Zhao Y, Bi Z, Jiang Q, et al. FTO regulates adipogenesis by controlling cell cycle progression via m6A-YTHDF2 dependent mechanism. Biochim Biophys Acta Mol Cell Biol Lipids. 2018;1863:1323–30.
34. Elbarbary RA, Lucas BA, Maquat LE. Retrotransposons as regulators of gene expression. Science. 2016;351:aac7247.
35. Karakülah G. RTFAdb: A database of computationally predicted associations between retrotransposons and transcription factors in the human and mouse genomes. Genomics. 2018;110:257–62.
36. Costanzo MC, von Grotthuss M, Massung J, Jang D, Caulkins L, Koesterer R, et al. The Type 2 Diabetes Knowledge Portal: an open access genetic resource dedicated to type 2 diabetes and related traits. Cell Metab. 2023;35:695-710.e6.
37. Sheinenzon A, Shehadeh M, Michelis R, Shaoul E, Ronen O. Serum albumin levels and inflammation. Int J Biol Macromol. 2021;184:857–62.
38. Musovic S, Olofsson CS. Adrenergic stimulation of adiponectin secretion in visceral mouse adipocytes is blunted in high-fat diet induced obesity. Sci Rep. 2019;9:1–12.
39. Jönsson ME, Garza R, Sharma Y, Petri R, Södersten E, Johansson JG, et al. Activation of endogenous retroviruses during brain development causes an inflammatory response. EMBO J. 2021;40:e106423.
40. Protasova MS, Andreeva TV, Rogaev EI. Factors regulating the activity of LINE1 retrotransposons. Genes. 2021;12:1562.
41. Ishiguro K, Kitajima H, Niinuma T, Maruyama R, Nishiyama N, Ohtani H, et al. Dual EZH2 and G9a inhibition suppresses multiple myeloma cell proliferation by regulating the interferon signal and IRF4-MYC axis. Cell Death Discov. 2021;7:1–13.
42. Di Giacomo M, Comazzetto S, Sampath SC, Sampath SC, O'Carroll D. G9a co-suppresses LINE1 elements in spermatogonia. Epigenetics Chromatin. 2014;7:1–7.
43. Banuelos-Sanchez G, Sanchez L, Benitez-Guijarro M, Sanchez-Carnerero V, Salvador-Palomeque C, Tristan-Ramos P, et al. Synthesis and characterization of specific reverse transcriptase inhibitors for mammalian LINE-1 retrotransposons. Cell Chem Biol. 2019;26:1095-1109.e14.
44. Takeuchi T, Kameyama K, Miyauchi E, Nakanishi Y, Kanaya T, Fujii T, et al. Fatty acid overproduction by gut commensal microbiota exacerbates obesity. Cell Metab. 2023;35:361-375.e9.
45. Wang X, Li Y, Chen W, Shi H, Eren AM, Morozov A, et al. Transcriptome-wide reprogramming of N6-methyladenosine modification by the mouse microbiome. Cell Res. 2019;29:167–70.
46. Jabs S, Biton A, Bécavin C, Nahori M-A, Ghozlane A, Pagliuso A, et al. Impact of the gut microbiota on the m6A epitranscriptome of mouse cecum and liver. Nat Commun. 2020;11:1344.
47. Van Hul M, Cani PD. The gut microbiota in obesity and weight management: microbes as friends or foe? Nat Rev Endocrinol. 2023;19:258–71.
48. Pan X-F, Chen Z-Z, Wang TJ, Shu X, Cai H, Cai Q, et al. Plasma metabolomic signatures of obesity and risk of type 2 diabetes. Obesity (Silver Spring). 2022;30:2294–306.
49. Kubo S, Sun M, Miyahara M, Umeyama K, Urakami K, Yamamoto T, et al. Hepatocyte injury in tyrosinemia type 1 is induced by

fumarylacetoacetate and is inhibited by caspase inhibitors. Proc Natl Acad Sci. 1998;95:9552–7.
50. Jacobs SMM, van Beurden DHA, Klomp LWJ, Berger R, van den Berg IET. Kidneys of mice with hereditary tyrosinemia type I are extremely sensitive to cytotoxicity. Pediatr Res. 2006;59:365–70.
51. Kim JK, Fillmore JJ, Sunshine MJ, Albrecht B, Higashimori T, Kim D-W, et al. PKC-θ knockout mice are protected from fat-induced insulin resistance. J Clin Invest. 2004;114:823–7.
52. Pan Y, Hui X, Hoo RLC, Ye D, Chan CYC, Feng T, et al. Adipocyte-secreted exosomal microRNA-34a inhibits M2 macrophage polarization to promote obesity-induced adipose inflammation. J Clin Invest. 2019;129:834–49.
53. Ji Y, Sun S, Xia S, Yang L, Li X, Qi L. Short term high fat diet challenge promotes alternative macrophage polarization in adipose tissue via natural killer T cells and interleukin-4 *. J Biol Chem. 2012;287:24378–86.
54. Kulenkampff E, Wolfrum C. Proliferation of nutrition sensing preadipocytes upon short term HFD feeding. Adipocyte. 2019;8:16–25.
55. Brestoff JR, Wilen CB, Moley JR, Li Y, Zou W, Malvin NP, et al. Intercellular mitochondria transfer to macrophages regulates white adipose tissue homeostasis and is impaired in obesity. Cell Metab. 2021;33:270-282.e8.
56. Choi WG, Choi W, Oh TJ, Cha H-N, Hwang I, Lee YK, et al. Inhibiting serotonin signaling through HTR2B in visceral adipose tissue improves obesity-related insulin resistance. J Clin Invest. 2021;131:e145331.
57. Lanciano S, Cristofari G. Measuring and interpreting transposable element expression. Nat Rev Genet. 2020;21:721–36.
58. Fresquet V, Garcia-Barchino MJ, Larrayoz M, Celay J, Vicente C, Fernandez-Galilea M, et al. Endogenous retroelement activation by epigenetic therapy reverses the Warburg effect and elicits mitochondrial-mediated cancer cell death. Cancer Discov. 2021;11:1268–85.
59. Sakashita A, Maezawa S, Takahashi K, Alavattam KG, Yukawa M, Hu Y-C, et al. Endogenous retroviruses drive species-specific germline transcriptomes in mammals. Nat Struct Mol Biol. 2020;27:967–77.
60. Hansen GT, Sobreira DR, Weber ZT, Thornburg AG, Aneas I, Zhang L, et al. Genetics of sexually dimorphic adipose distribution in humans. Nat Genet. 2023;55:461–70.
61. Rubio K, Molina-Herrera A, Pérez-González A, Hernández-Galdámez HV, Piña-Vázquez C, Araujo-Ramos T, et al. EP300 as a molecular integrator of fibrotic transcriptional programs. Int J Mol Sci. 2023;24:12302.
62. Rafehi H, Kaspi A, Ziemann M, Okabe J, Karagiannis TC, El-Osta A. Systems approach to the pharmacological actions of HDAC inhibitors reveals EP300 activities and convergent mechanisms of regulation in diabetes. Epigenetics. 2017, Available from: https://www.tandfonline.com/doi/abs/10.1080/15592294.2017.1371892. Cited 7 Dec 2024.
63. Hwang Y-J, Lee E-W, Song J, Kim H-R, Jun Y-C, Hwang K-A. MafK positively regulates NF-κB activity by enhancing CBP-mediated p65 acetylation. Sci Rep. 2013;3:3242.
64. Xue W, Huang J, Chen H, Zhang Y, Zhu X, Li J, et al. Histone methyltransferase G9a modulates hepatic insulin signaling via regulating HMGA1. Biochim Biophys Acta Mol Basis Dis. 2018;1864:338–46.
65. Lee RA, Chang M, Yiv N, Tsay A, Tian S, Li D, et al. Transcriptional coactivation by EHMT2 restricts glucocorticoid-induced insulin resistance in a study with male mice. Nat Commun. 2023;14:3143.
66. Zhang W, Yang D, Yuan Y, Liu C, Chen H, Zhang Y, et al. Muscular G9a regulates muscle-liver-fat axis by musclin under overnutrition in female mice. Diabetes. 2020;69:2642–54.
67. Wang L, Xu S, Lee J, Baldridge A, Grullon S, Peng W, et al. Histone H3K9 methyltransferase G9a represses PPARγ expression and adipogenesis. EMBO J. 2013;32:45–59.
68. Able AA, Richard AJ, Stephens JM. TNFα effects on adipocytes are influenced by the presence of lysine methyltransferases, G9a (EHMT2) and GLP (EHMT1). Biology. 2023;12:674.
69. Scheer S, Zaph C. The lysine methyltransferase G9a in immune cell differentiation and function. Front Immunol. 2017 8. Available from: https://www.frontiersin.org/journals/immunology/articles/10.3389/fimmu.2017.00429/full. Cited 7 Dec 2024.
70. Norman BP, Davison AS, Hughes JH, Sutherland H, Wilson PJM, Berry NG, et al. Metabolomic studies in the inborn error of metabolism alkaptonuria reveal new biotransformations in tyrosine metabolism. Genes Dis. 2022;9:1129–42.
71. Kim J, Lee G. Metabolic control of m6A RNA modification. Metabolites. 2021;11:80.
72. Rønningen T, Dahl MB, Valderhaug TG, Cayir A, Keller M, Tönjes A, et al. m6A regulators in human adipose tissue - depot-specificity and correlation with obesity. Front Endocrinol (Lausanne). 2021;12:778875.
73. Turcot V, Tchernof A, Deshaies Y, Pérusse L, Bélisle A, Marceau S, et al. LINE-1 methylation in visceral adipose tissue of severely obese individuals is associated with metabolic syndrome status and related phenotypes. Clin Epigenetics. 2012;4:10.
74. Pan X-F, Chen Z-Z, Wang TJ, Shu X, Cai H, Cai Q, et al. Plasma metabolomic signatures of obesity and risk of type 2 diabetes. Obesity. 2022;30:2294–306.

Publisher's Note